

Procédure expérimentale

Dans ce chapitre sont présentés la méthode d'extraction du ^{10}Be dans les échantillons de glace, le principe de mesure par AMS, ainsi que les incertitudes et les corrections associées.

4.1 Préparation des échantillons

4.1.1 Extraction chimique du béryllium

La glace pour cette étude était sous la forme de « bag », c'est-à-dire une série continue coupée tous les 55 cm. Des améliorations dans la préparation chimique des échantillons et dans le système de mesure par spectrométrie de masse par accélérateur (AMS) ont été apportées depuis les premières expérimentations [Raisbeck et al., 1978, 1987; Yiou et al., 1997]. L'extraction du béryllium de la glace ainsi que la mise en cathode des échantillons (e.g. section 4.1.2) se déroulaient au Centre de Spectrométrie Nucléaire et de Spectrométrie de Masse (CSNSM). La méthode actuelle est décrite de manière détaillée par Raisbeck et al. [2007]. L'échantillon de glace (11 cm) est tout d'abord fondu en présence de 0,25 mg de ^9Be (sous forme d'une solution $^9\text{Be} + \text{eau déionisée}$) qui sert d'entraîneur afin de pouvoir mesurer le rapport $^{10}\text{Be}/^9\text{Be}$ de l'échantillon. Une fois l'échantillon sous forme liquide, le béryllium est précipité sous forme $\text{Be}(\text{OH})_2$ à l'aide de 50 μL d'ammoniac NH_4OH (le béryllium précipite quand le pH de la solution est basique). Le précipité est ensuite extrait par centrifugation et dissous dans 250 μL d'acide nitrique et 500 μL d'eau ultra-purifiée, puis introduit dans un creuset en céramique pour être séché sur une plaque chauffante. Une fois sec, le précipité est chauffé à 900°C durant 45 minutes afin d'obtenir environ 0,6 mg d'oxyde de béryllium (BeO). Des blancs chimiques, c'est-à-dire des échantillons dont la glace est remplacée par de l'eau déionisée, ont

aussi été préparés suivant la même méthode afin d'évaluer une contamination éventuelle de l'entraîneur ou matériel utilisé pour l'extraction du ^{10}Be .

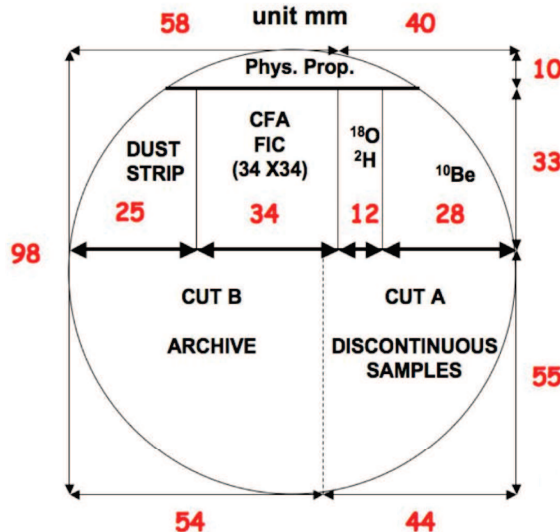


FIGURE 4.1 – Coupe transversale d'une carotte de glace montrant la fraction utilisée pour la mesure du ^{10}Be .

Transversal cut of an ice core showing the part used for the ^{10}Be measurements.

4.1.2 Mise en cathode

La poudre d'oxyde de beryllium peut ensuite être mélangée avec de la poudre de niobium (Nb). Celle-ci permet d'améliorer la conduction de l'échantillon dans la source du spectromètre, et ainsi améliorer le rendement d'extraction des ions. La poudre de Nb est donc introduite dans le creuset en céramique et incorporée à l'échantillon à l'aide d'une spatule, ceci afin d'obtenir un mélange homogène. Ce mélange est introduit à l'aide d'un entonnoir dans une cathode en cuivre qui est ensuite mise sous presse dans le but de compacter la poudre dans la cible. Les ustensiles de travail sont nettoyés à l'éthanol entre chaque échantillon. Le rapport $^{10}\text{Be}/^{9}\text{Be}$ de chaque cathode est mesuré par AMS au Centre Européen de Recherche et d'Enseignement des Géosciences de l'Environnement (CEREGE), à Aix-en-Provence.

4.2 Mesure des rapports $^{10}\text{Be}/^{9}\text{Be}$ par spectrométrie de masse par accélérateur

4.2.1 Description de l'AMS

Les mesures présentées dans ce manuscrit ont été réalisées sur l'accélérateur tandem ASTER (Accélérateur pour les Sciences de la Terre, Environnement, Risques) installé au CEREGE [Klein et al., 2008]. Son principe est le même que celui d'un spectromètre de masse classique. Il est composé d'une source, d'un accélérateur de 5 MV de type tandem avec deux étapes d'accélération (qui constitue la différence majeure avec des spectromètres de masse dits conventionnels), d'aimants pour la séparation magnétique, et d'un système de détection. Une photo ainsi qu'un schéma de fonctionnement de l'AMS sont représentés sur la Fig. 4.2. Une haute énergie est nécessaire pour la mesure du ^{10}Be dans nos échantillons car il n'est pas assez abondant pour être détecté par un spectromètre de masse classique. Concernant le ^{10}Be , un des points critiques est la présence en abondance de son isobare le bore-10 (^{10}B). Tout le cheminement d'une mesure, de la source au détecteur en passant par l'élimination du ^{10}B , est expliqué ci-dessous en se référant aux étapes annotées dans la Fig. 4.2b.

Les cathodes sont placées dans un carrousel permettant de lancer 200 analyses. Le carrousel est ensuite chargé au niveau de la source ionique (1), une chambre sous vide dans laquelle est injectée du césium neutre sous forme de vapeur. Le césium est ionisé à haute température (Cs^+) par ionisation de surface afin de bombarder la cible et de produire des ions moléculaires négatifs BeO^- , qui sont extraits grâce à une différence de potentiel entre la cible et l'extracteur à la sortie de la source, focalisés et transportés vers l'aimant d'injection (2). Le faisceau BeO^- passe donc à travers le premier aimant. Pour un ion de masse m , de charge q ($q = ze$, z étant le nombre de charges élémentaires e de l'ion), et de vitesse v dans un champ magnétique homogène B , sa trajectoire circulaire r suit l'équation :

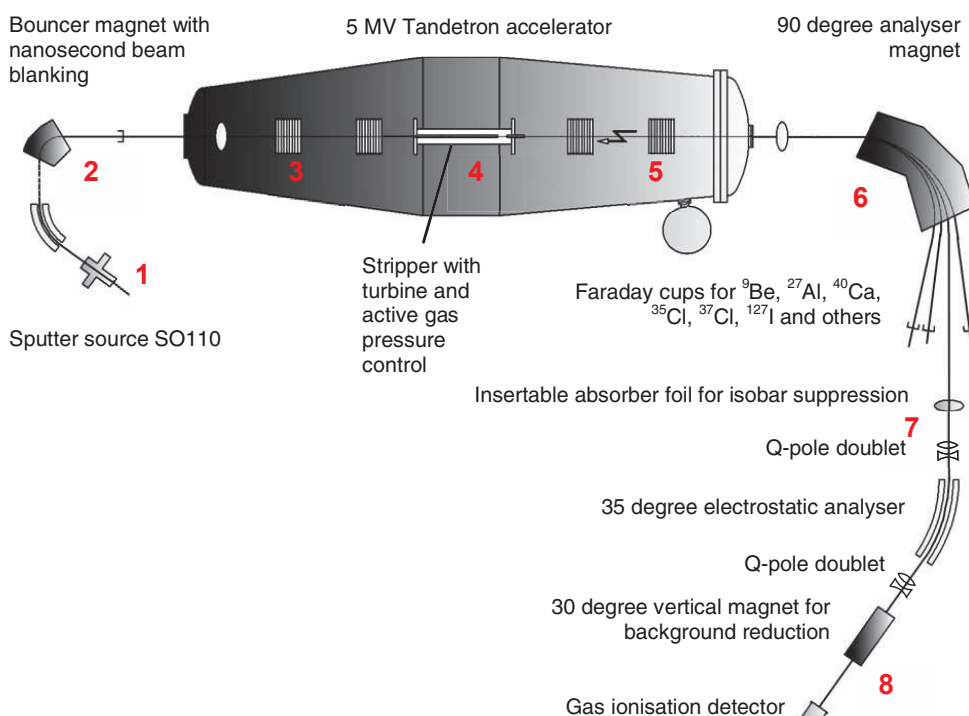
$$r = \frac{mv}{qB} \quad (4.1)$$

Le rayon de la trajectoire des ions est donc proportionnel au rapport de leur quantité de mouvement mv sur leur charge q . Dans ce premier aimant, les ions $^{10}\text{BeO}^-$ (masse 26) et $^9\text{BeO}^-$ (masse 25) sont alternativement sélectionnés avec une résolution de l'ordre de la nanoseconde [Klein et al., 2008] afin d'être injectés dans l'accélérateur tandem du système AMS (3). Le faisceau d'ions est ici accéléré dans un premier tube

accélérateur. Des résistances montées directement sur le périmètre des électrodes



(a)



(b)

FIGURE 4.2 – (a) Installation ASTER au CEREGE. (b) Schéma de l'AMS 5 MV au CEREGE [Klein et al., 2008].

(a) ASTER installation at CEREGE. (b) Layout of the 5 MV AMS system in the CEREGE [Klein et al., 2008].

du tube distribuent le potentiel de manière homogène tout le long de ce parcours [Gottdang et al., 2002]. Le faisceau atteint le « gaz éplucheur » (stripper, 4) qui est ici du gaz argon à faible pression. En passant à travers le gaz, les ions moléculaires négatifs sont « cassés », formant des ions atomiques qui sont convertis en ions positifs dus à la perte d'électrons (Be^+ , Be^{2+} , Be^{3+} , Be^{4+} , les ions majoritaires ayant une charge 2+). Cette étape permet également la destruction des molécules isobares. Ils sont ensuite accélérés dans la seconde moitié de l'unité d'accélération (5). À la

4.2. Mesure des rapports $^{10}\text{Be}/^{9}\text{Be}$ par spectrométrie de masse par accélérateur

sortie, le faisceau d’ions possède une très grande énergie. Le faisceau est ensuite dirigé vers un nouvel aimant (6) afin de séparer les masses 9 et 10. Au sortir de l’aimant, les ions $^{9}\text{Be}^{2+}$ sont détectés par mesures des courants électriques collectés dans des cages de Faraday, alors que les ions $^{10}\text{Be}^{2+}$ doivent être séparés de leur isobare le ^{10}B . Pour cela, une feuille de nitre de silicium (Si_3N_4) est placée sur leur trajectoire (7) à l’entrée d’un déflecteur électrostatique, provoquant une perte d’énergie différentielle des ions [Raisbeck et al., 1984; Nottoli et al., 2013], suivant la formule de Bethe-Bloch dans un cas non-relativiste [Beer et al., 2012] :

$$\frac{dE}{dx} \propto \frac{mz^2}{E} \quad (4.2)$$

La quantité d’énergie perdue étant proportionnelle au numéro atomique, la perte d’énergie du ^{10}B ($z = 5$) est plus importante que celle du ^{10}Be ($z = 4$). En effet après cette étape, le ^{10}Be a perdu environ 0,9 MeV de son énergie et sa différence relative en énergie avec le ^{10}B est d’environ 4% [Klein et al., 2008]. De cette manière, le ^{10}Be et son isobare ^{10}B peuvent être séparés de manière efficace. Ce processus de séparation n’est possible qu’à très haute énergie. Durant cette procédure, des électrons sont arrachés rendant l’ion $^{10}\text{Be}^{4+}$ majoritaire. Le déflecteur électrostatique qui suit supprime le ^{10}B par un facteur d’au moins 10^5 . L’aimant placé derrière réduit le bruit de fond provoqué par l’éparpillement de ions au niveau des électrodes du déflecteur [Klein et al., 2008]. Le faisceau est finalement dirigé vers le détecteur à gaz d’ionisation (8) qui mesure la perte d’énergie des ions par unité de distance à travers le gaz (technique dE/dx) afin de finaliser la séparation du ^{10}Be et du ^{10}B . La pression du gaz est réglée de façon à ce qu’un atome de ^{10}Be traverse tout le détecteur alors qu’un atome de ^{10}B est arrêté au niveau du premier compteur. La mesure est déclenchée par l’arrivée des ions dans le second compteur.

4.2.2 Corrections et incertitudes

Les rapports $^{10}\text{Be}/^{9}\text{Be}$ des échantillons sont mesurés relativement à celui d'un matériel standard de rapport isotopique connu, le NIST SRM 4325* d'une valeur connue $^{10}\text{Be}/^{9}\text{Be} = 2,68 \cdot 10^{-11}$. Ce standard est mesuré plusieurs fois durant un run de mesures, ceci afin de prendre en compte la dérive de la machine et la distribution des états de charges après le passage à travers la feuille de Si_3N_4 . Celui-ci permet de corriger le rapport mesuré des échantillons grâce à un facteur correctif (ratio entre le rapport mesuré du standard et sa valeur réelle). Durant un run de mesures de ^{10}Be sont mesurés par l'AMS ASTER : quatre cibles-référence NIST SRM 4325, un blanc machine (solution commerciale d'entraîneur ^{9}Be directement précipitée), et les échantillons sur les positions restantes (comprenant aussi quelques blancs chimiques). Durant un batch (mesure de tous les échantillons sur la roue), chaque cible subit trois passages de 200 coups chacun, soit environ 6 minutes pour les échantillons de glace. Ce nombre de coups conduit typiquement à une incertitude statistique de l'ordre de 4% pour un écart-type à 1σ . Le rapport moyen mesuré des 21 blancs chimiques régulièrement produits durant la préparation des échantillons est de $(3,95 \pm 2,35) \times 10^{-15}$. Le bruit de fond est évalué grâce aux blancs machine. [Arnold et al. \[2010\]](#) ont mesuré une valeur moyenne de $(0,6 \pm 0,3) \times 10^{-15}$ sur 90 blancs machine. En comparaison, les échantillons mesurés dans le cadre de cette thèse (2200 échantillons entre 2384 et 2627 m de profondeur à EDC) ont un rapport moyen $^{10}\text{Be}/^{9}\text{Be}$ de $3,2 \times 10^{-13}$.

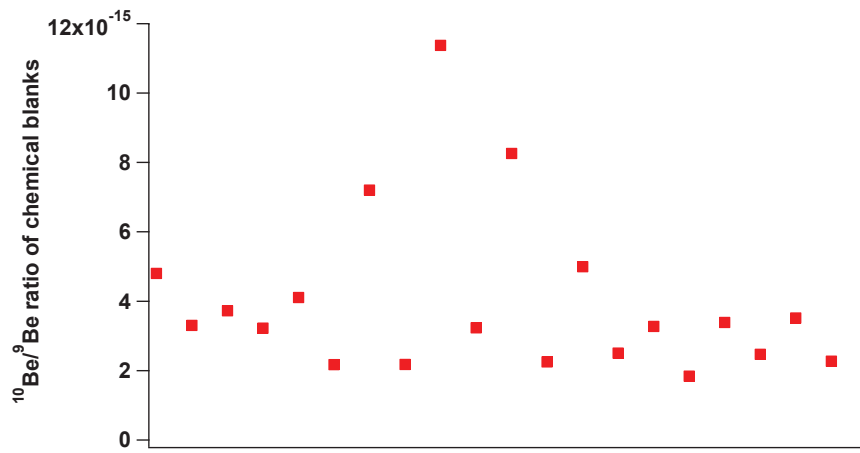
4.2.3 Calcul des concentrations en ^{10}Be

Les mesures obtenues grâce à l'AMS sont des rapports $^{10}\text{Be}/^{9}\text{Be}$ qu'il faut convertir en concentrations de ^{10}Be . Pour cela, plusieurs informations sont nécessaires : la quantité de ^{9}Be ajoutée lors de la préparation de l'échantillon (250 μL d'une solution aqueuse contenant 1 g/L de ^{9}Be , soit 0,25 mg) et la masse de l'échantillon de glace. La concentration en ^{10}Be est calculée selon la formule :

$$\left[^{10}\text{Be} \right]_{at/g} = \frac{^{10}\text{Be}}{^{9}\text{Be}} \Big|_{\text{échantillon}} \times \frac{\mathcal{N}_A \times (m_{^{9}\text{Be}}/M_{^{9}\text{Be}})}{m_{glace}} \quad (4.3)$$

où \mathcal{N}_A est le nombre d'Avogadro ($6,02214 \cdot 10^{23} \text{ mol}^{-1}$), $m_{^{9}\text{Be}}$ la masse de ^{9}Be ajouté lors de la préparation de l'échantillon (0,25 mg), $M_{^{9}\text{Be}}$ la masse molaire du ^{9}Be ($9,012 \text{ mol.g}^{-1}$) et m_{glace} la masse de l'échantillon de glace analysé. L'incertitude sur la valeur du rapport $^{10}\text{Be}/^{9}\text{Be}$ est propagée sur le calcul des concentrations. Il

*. NIST : National Institute of Standards and Technology. SRM : Standard Reference Material.



High resolution 10Be record in EPICA Dome C ice core over a whole climatic cycle (MIS 9)

Currently, the time series of ^{10}Be available focus on the Holocene or during geomagnetic events like the Laschamp excursion or the Matuyama-Brunhes reversal which is, until now, the only published period beyond the last glacial-interglacial cycle. 2200 ^{10}Be samples on the EPICA Dome C ice core between 2384 and 2627 m deep have been prepared and measured in the framework of this PhD, allowing to discuss the first high resolution ^{10}Be record on a whole climatic cycle. Covering the period between 355 and 269 kyr BP (EDC3 age scale), this time series includes the Termination IV and the interglacial period MIS 9 where the resolution of our ^{10}Be profile reaches \sim 20 years. Such a high resolution is very interesting for the study of the influence of solar activity (like the de Vries or Gleissberg cycles) and the comparison with the current interglacial period. It is also possible to test the robustness of ^{10}Be flux shown in this chapter with respect to the uncertainties linked to the accumulation rate of the site, the chronology, the climate and the transport and deposition processes. The results presented in this chapter will be submitted for publication in the form of two separate articles. One is centered on the solar activity during the interglacial period MIS 9.3, the other concerns the informations which can be deduced from climatic reconstructions (temperature and accumulation information).

5.1 Introduction

The cosmogenic isotope beryllium-10 (^{10}Be), with a half-life of 1.39×10^6 years [Korschinek et al., 2010], is produced in the upper atmosphere by the interaction of Galactic Cosmic Rays (GCR) with nitrogen and oxygen [Lal and Peters, 1967]. Because GCR are modulated by geomagnetic and heliomagnetic fields, records of ^{10}Be provide useful information about past variations in solar activity and geomagnetic field intensity. As a consequence, the higher the solar or geomagnetic field, the more primary cosmic ray particles are deflected, which leads to a decrease of cosmogenic isotope production. After their production, ^{10}Be atoms become fixed to aerosols and fall very quickly (within \sim 1-2 years according to Raisbeck et al. [1981a]) on the Antarctic plateau primarily by dry deposition. The stratosphere contributes the most to the total production (67% according to Lal and Peters [1967], 56% according to Masarik and Beer [1999], and 65% according to Heikkilä et al. [2009]). One important question is to know if the ^{10}Be measured in the ice cores represents a global signal (because principally ^{10}Be is well-mixed in the stratosphere [Heikkilä et al., 2008]) or if there is a polar bias [Bard et al., 1997; Field et al., 2006] due to latitudinal dependence of the production of ^{10}Be (maximum ^{10}Be production at polar latitudes ($\geq 65^\circ$) and minimum ^{10}Be production at the equator [Masarik and Beer, 1999, 2009; Kovaltsov and Usoskin, 2010]).

^{10}Be has been particularly studied in ice cores from Greenland [Beer et al., 1988, 1990; Finkel and Nishiizumi, 1997; Yiou et al., 1997; Wagner et al., 2001; Muscheler et al., 2004, 2005] and Antarctica [Yiou et al., 1985; Raisbeck et al., 1987, 1990, 1992, 2006; Dreyfus et al., 2008; Horiuchi et al., 2008; Baroni et al., 2011], as in sediments [Raisbeck et al., 1985; Robinson et al., 1995; Ménabréaz et al., 2011, 2012; Nilsson et al., 2011]. ^{10}Be is a useful tool to study distinctive features, such as the Laschamp excursion [Raisbeck et al., 2007; Nilsson et al., 2011; Ménabréaz et al., 2011, 2012] or the Matuyama-Bruhnes inversion [Raisbeck et al., 2006; Dreyfus et al., 2008], providing stratigraphic markers helpful for the datation of cores. One advantage of ice cores is that they offer a relatively simple way to calculate ^{10}Be fluxes from the measured concentration ^{10}Be and the estimated ice accumulation rate, better constrained than for marine sediments. Moreover, ^{10}Be falls mainly by dry deposition on this site, so that one can suppose in all likelihood that ^{10}Be flux in sites on the Antarctic plateau, like Dome C, represents the atmospheric concentration [Alley et al., 1995; Finkel and Nishiizumi, 1997], so the ^{10}Be production. Finally, the high resolution of ice cores gives access to the study of shorter events due to solar activity for example [Beer et al., 1990; Wagner et al., 2001; Baroni et al., 2011].

The solar activity, expressed as the sunspot numbers, has been recorded consis-

tently since 1843, when Schwabe discovered the 11-yr cycle. Especially, the commencement of the “instrumental” era in 1936 with the use of ionisation chambers and then neutron monitor measurements has brought very precise data about solar activity [McCracken, 2007]. Earlier data can be reconstructed from historical documents mentioning sunspot activity, but the data before 1600 become more and more incomplete and uncertain [Beer et al., 1990]. One way to overcome this problem is to study cosmogenic isotopes which are proxies of solar activity. Since several decades, numerous records of ^{14}C and ^{10}Be have allowed to detect decadal or centennial variability linked to solar activity according to the time domain of the studies. The famous 11-yr cycle has been detected by Beer et al. [1990] and Baroni et al. [2011] in ^{10}Be from ice cores. Past millennial solar activity, including events as the Maunder or the Spörer minimum has been studied using ^{10}Be in ice core [Raisbeck et al., 1990; Horiuchi et al., 2008] and ^{14}C in tree rings [Bard et al., 1997]. Until now, the Holocene (past 10000 years) is the only period where temporal studies of solar activity are available for centennial variability, except for unusual events as during the Lachamp excursion [Wagner et al., 2001]. Indeed, the de Vries cycle (~ 200 years) has been detected during the Holocene in tree rings ^{14}C [Suess, 1980; Reimer et al., 2004, 2009] and in ^{10}Be from the Greenland and Antarctica ice cores [Raisbeck et al., 1990; Vonmoos et al., 2006; Steinhilber et al., 2012], and during the Laschamp event [Wagner et al., 2001].

Particularly relevant to our current work, is the recent study made recently by Steinhilber et al. [2012]; using principal component analysis (PCA), these authors have combined different ^{10}Be ice core records from Greenland and Antarctica with the global ^{14}C tree ring record [Reimer et al., 2009] over the Holocene period. Considering this composite curve as a cosmic-ray induced production signal (and so a proxy for solar activity), they found periodic variations such as the de Vries cycle. Based on the agreement between the spectral characteristics of this composite curve and of the planetary torque, these same data have been used to put forward the idea that the long-term solar magnetic activity is modulated by planetary effects [Abreu et al., 2012].

Hereafter, we present a new high resolution ^{10}Be profile measured along the EPICA Dome C ice core ($75^\circ 06' \text{S}, 123^\circ 21' \text{E}$) from 2384 to 2627 m deep. Based on the EDC3 age scale [Parrenin et al., 2007b], this record covers the period between 269 and 355 kyr BP (thousand of years Before Present) from Marine Isotope Stages (MIS) 8 to 10 including Termination IV and MIS 9. Our depth resolution being constant (11 cm), we have a higher time resolution for the period of higher accumulation, e.g. for MIS 9.3, the warmest part of MIS 9 [Jouzel et al., 2007] where

it reaches \sim 20 years. While measurements correspond to ^{10}Be concentration, interpretation is based on ^{10}Be flux which also depends on snow accumulation. We examine the multidecadal record over which we do not observe flux changes such as the peak associated with the Laschamp event 41 kyr ago [Raisbeck et al., 2007]. Then, we test the influence of climate and atmospheric transport on the variability of our ^{10}Be flux record. We also discuss how this \sim 75 kyr long record allows to infer information about the associated glacial–interglacial temperature change, from the observed link between ^{10}Be , accumulation rate and deuterium. Finally, we focus on the highly detailed MIS 9.3 record and how its spectral properties compare with the Holocene in the light of recent studies of solar activity during the Holocene [Steinhilber et al., 2012; Abreu et al., 2012].

5.2 Results

Here we present the ^{10}Be data from EPICA Dome C ice core between 2384 and 2627 m deep (from 269 to 355 kyr BP with EDC3 age scale). The preparation and measurement processes are detailed in the section 4.1. Fig. 5.1 shows high resolution profile of ^{10}Be concentrations and fluxes. The time resolution for this period varies between 20 years for the interglacial MIS 9.3 period and 70 years for the glacial period older than 340 kyr BP (see Fig. 5.1d). ^{10}Be reaches the Antarctic plateau primarily by dry deposition. For dry deposition sites as EDC, climatic component can be minimized by calculating the ^{10}Be flux (concentration \times accumulation rate \times ice density). Indeed, it is a more appropriate parameter to study production variations [Raisbeck et al., 1992; Alley et al., 1995; Finkel and Nishiizumi, 1997].

Results are shown using the EDC3 timescale derived by Parrenin et al. [2007b]. It has been developed combining an accumulation model and an ice flow model using an inverse method to estimate the free parameters of this model in such a way to optimize the timescale with respect to prescribed time markers [Parrenin et al., 2007a]. Derived assuming an exponential link with δD (see Fig. 5.1a and 5.1b) the accumulation shows an anti-correlation with the measured ^{10}Be concentrations as previously pointed out for Antarctic cores [Yiou et al., 1985; Jouzel, 1989; Raisbeck et al., 1992]. Resulting raw and low-pass filtered ($1/2000 \text{ yr}^{-1}$) ^{10}Be fluxes are shown on Fig. 5.1c ; δD is also included in this graph (grey curve on Fig. 5.1b from Jouzel et al. [2007]). The low-pass filtered ^{10}Be flux does not show large excursion but several millennial changes can be observed between 303 and 279 kyr BP (e.g. minima of these variations showing by the arrows in Fig. 5.1). The curve displays first a great minimum of ^{10}Be flux at 303 kyr BP followed by a long increase during

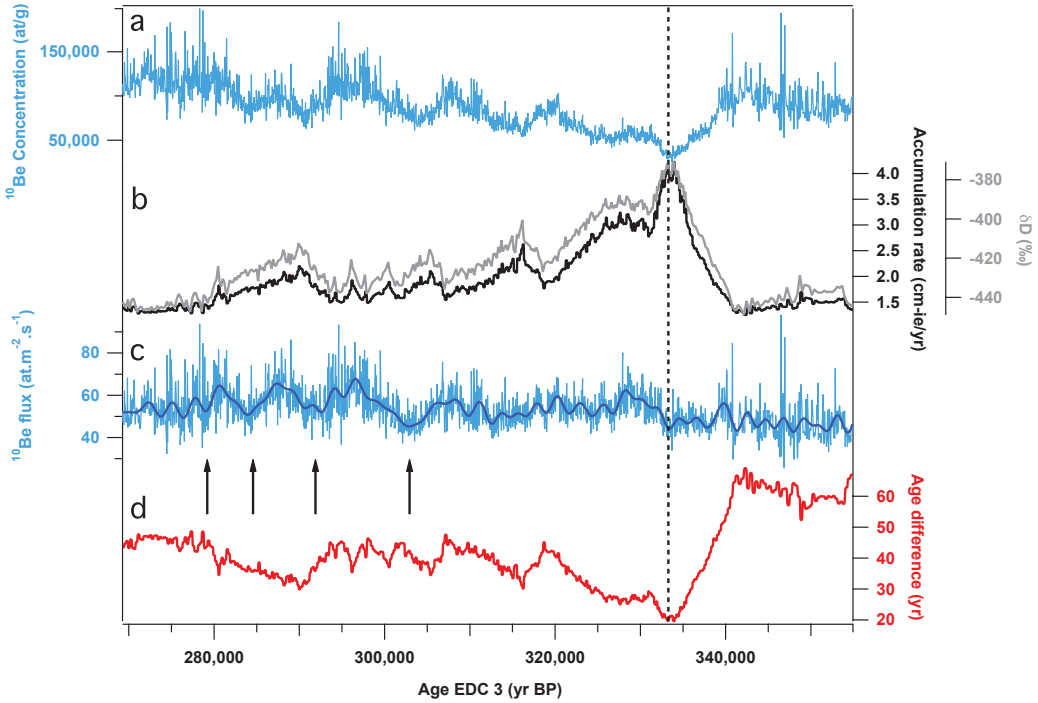


Figure 5.1: High resolution ^{10}Be data between 2384 and 2627 m deep (269 – 355 kyr BP on EDC3 age scale). (a) Raw ^{10}Be concentrations (at/g). (b) In black, the accumulation rate of the site ($\text{cm-}^{\text{ie}}/\text{yr}$). In grey, δD profile at EDC including the interglacial period MIS 9.3. (c) Calculated ^{10}Be flux using EDC3 accumulation rate. The light-blue curve corresponds to raw data, the bold-blue curve is the low-pass filtered ^{10}Be flux ($1/2000 \text{ yr}^{-1}$). The arrows show the minima of millennial variations described in section 5.2. The dotted line corresponds to the minimum in ^{10}Be flux, coincident with the maximum of accumulation. (d) Resolution of the ^{10}Be profile (difference between the n and $n+1$ sample ages).

~ 6000 years. The next minima are reached at 292, 284 and 279 kyr BP (noted by the arrows in Fig. 5.1). These variations appear during a stable glacial period, with no change of δD . During the older period (between 340 and 355 kyr BP), ^{10}Be flux is quite stable and on average lower ($\sim 47.5 \text{ at.m}^{-2}.\text{s}^{-1}$ against a global average of $53.44 \text{ at.m}^{-2}.\text{s}^{-1}$). The minimum of ^{10}Be flux is highlighted by the dotted line. It matches with the maximum of accumulation rate during the MIS 9. We have performed spectral analyses with ^{10}Be flux (Fig. 5.2a: blue curve on the Fourier analysis; Fig. 5.2b: wavelet analysis). The most important signal is a significant period of ~ 10500 years corresponding to the millennial variations described above.

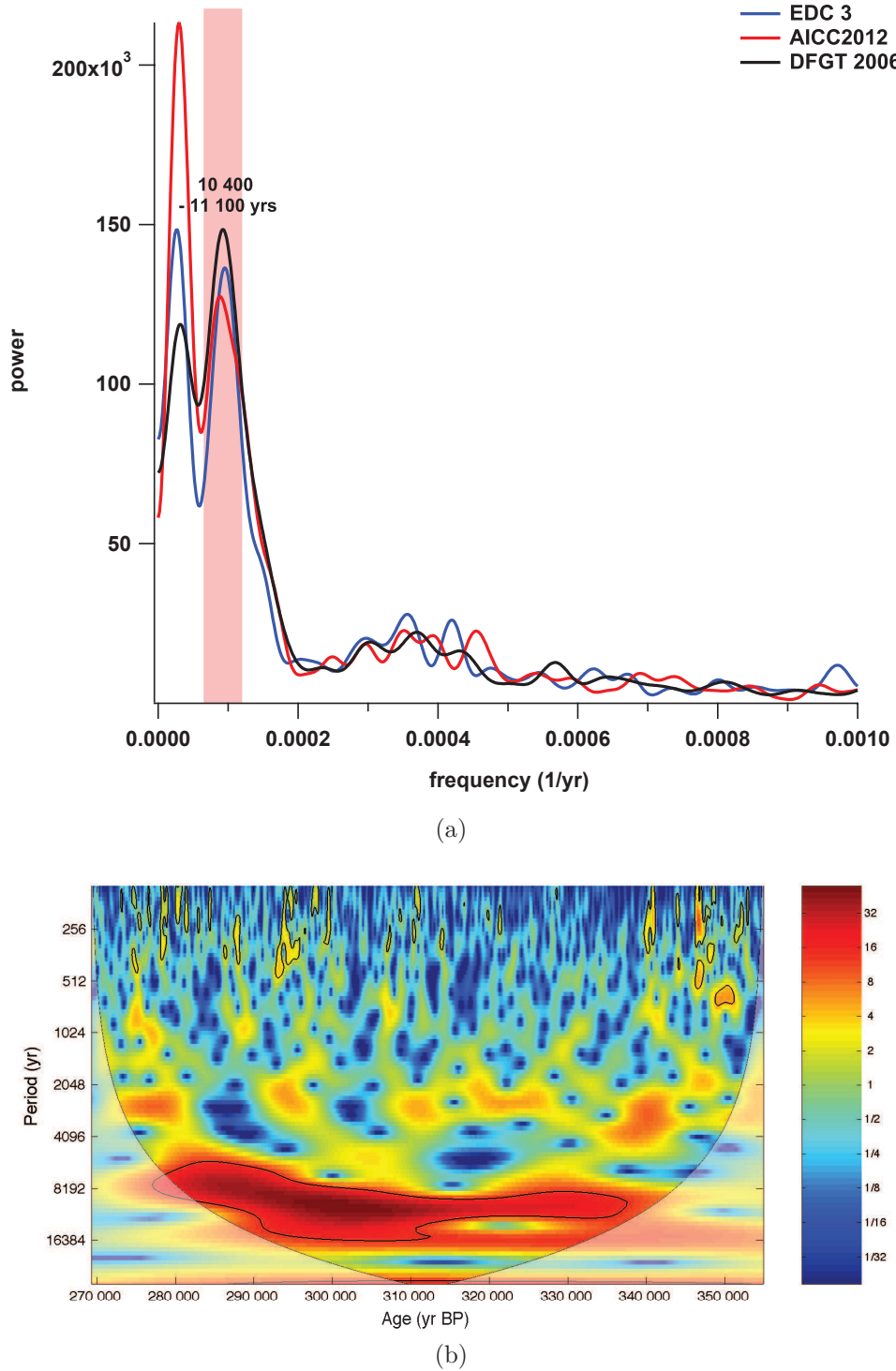


Figure 5.2: Spectral analyses of ^{10}Be flux between 269 and 355 kyr BP. (a) Fourier analysis on ^{10}Be for three different age scales: EDC3 in blue, AICC2012 in red and DFGT-2006 in black. The common period (~ 10500 years) is highlighted in light red. (b) Wavelet analysis of ^{10}Be flux on the EDC3 age scale. The same ~ 10500 years cycle, highlighted in the Fourier analysis, is detected as well as some centennial variabilities.

5.3 Causes of millennial variations of ^{10}Be flux

5.3.1 Climatic influence

It is unlikely that the millennial variability identified in the ^{10}Be spectra is due climatic variations as suggested from the comparison of the ^{10}Be flux and δD wavelet spectra calculated using the squared wavelet coherence (WTC) reported on the Fig. 5.3. The WTC can be defined as a localized correlation coefficient in time frequency space (see section C.1 in the appendix for the description of the wavelet package from [Grinsted et al. \[2004\]](#)). No significant correlation is observed between these two

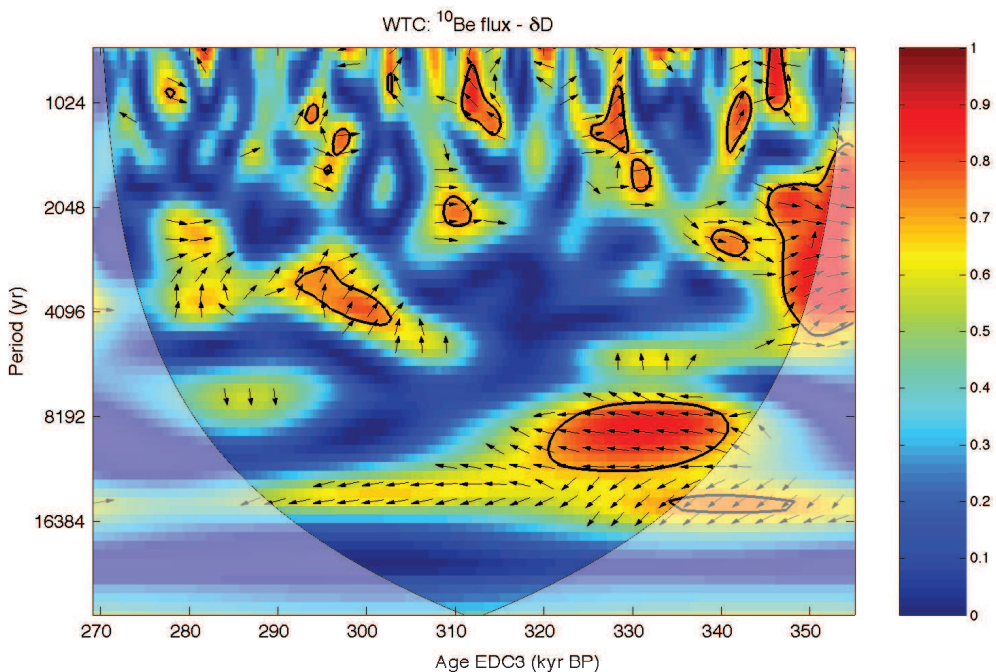


Figure 5.3: Squared wavelet coherence (WTC) of the ^{10}Be flux and δD spectrums. It can be defined as a local cross-correlation. No evident correlation is detected, except a significant region during the MIS 9.3 with an anti-phase relationship for a period of ~ 9000 years, but not linked with climatic effects (see section 5.3.1).

variables during this climatic cycle at EDC ($r = 0.0595$ with 95% confidence interval [0.0035 ; 0.1152]). The WTC of ^{10}Be flux and δD allows us to investigate the correlations between both signals more locally. Again, no correlation is detected, except a significant region during the MIS 9.3 with an anti-phase relationship between ^{10}Be and δD for a period of ~ 9000 years. This period corresponds to the time interval where δD , and hence accumulation rate, varies more significantly. This probably means that this anti-correlation is an artifact due to the estimate of accumulation rate from δD during the studied period and not the presence of a climatic compo-

nent in the ^{10}Be flux. For the shorter periods, significant regions are very sparse without a dominant mean phase angle. Periods shorter than 1200 years cannot be considered because of the resampling applied on ^{10}Be and δD data (~ 345 years).

5.3.2 Transport and deposition effects

Because ^{10}Be atoms are likely attached to aerosols after their production, they can be influenced by transport and deposition effects before their trapping in the ice. We study here their influence on the millennial variations of our measured ^{10}Be signal via a comparison with a record of aerosols concentration, that is high resolution sulfate data at EDC [Traversi et al., 2009]. Sulfate record has been resampled to the resolution of our ^{10}Be measurements (11 cm) before calculating its flux (in $\text{ng} \cdot \text{m}^{-2} \cdot \text{s}^{-1}$) in the same way than for ^{10}Be (Fig. 5.4).

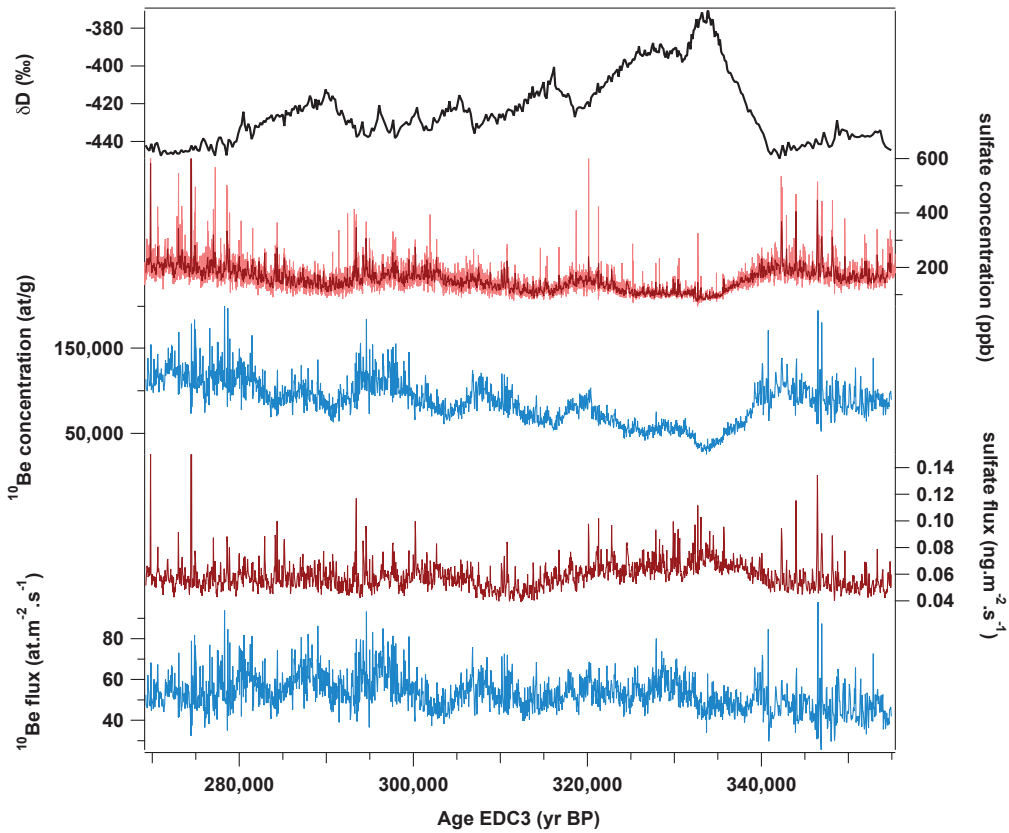


Figure 5.4: Comparison of our ^{10}Be measurements with sulfate data from Traversi et al. [2009]. From top to bottom, δD from EDC, raw sulfate concentrations in ppb (light red) and 11 cm resample sulfate concentrations (brown), ^{10}Be concentrations, sulfate flux ($\text{ng} \cdot \text{m}^{-2} \cdot \text{s}^{-1}$), and ^{10}Be flux.

The correlation coefficient between ^{10}Be and SO_4^{2-} moves from $r = 0.65$ (with

95% confidence interval [0.6278 ; 0.6758]) for the concentrations profiles to $r = 0.1165$ (with 95% confidence interval [0.0751 ; 0.1575]) for the flux. We indeed directly observe that there are no common millennial variations in our ^{10}Be profile and in the SO_4^{2-} flux record. This means that the millennial changes in our ^{10}Be profile cannot be mainly explained transport and deposition effects, but come from another source.

5.3.3 Dating uncertainties

To test the sensitivity of ^{10}Be changes to chronology, we compare by spectral analysis ^{10}Be flux on three different age scales: the conventional EDC3 age scale, DFGT–2006 age scale from Dome Fuji [[Kawamura et al., 2007; Parrenin et al., 2007a,b](#)] and the new multi-proxy chronology AICC2012 [[Bazin et al., 2013](#)]. The comparison of the different ^{10}Be flux spectra on the three different chronologies (top of the Fig. 5.2) shows that the most significant period of ~ 10500 years, and so the millennial changes of ^{10}Be flux, are not affected by chronology.

5.4 Validity of the interpretation of glacial–interglacial accumulation and temperature change in the EDC ice core

It is interesting to test the assumption of a strictly constant ^{10}Be flux, consequences on the accumulation rate variations and whether or not it allows to keep the EDC chronology consistent with the ascribed time markers. Over this period, the time markers for the EDC ice core are deduced from total air content aligned with an integrated summer insolation curve [[Raynaud et al., 2007](#)]. To examine the impact of the assumption of ^{10}Be flux on the chronology we have used using the bayesian dating tool Datice [[Lemieux-Dudon et al., 2010](#)]. Fig. 5.5 shows the accumulation rate curves after the processing by Datice to obtain the best compromise between the background chronology (built from the proposed accumulation rate and the thinning obtained by glaciological modeling) and observations (age markers). The Datice tool easily converges towards the prescribed age markers. Such a result is not surprising since our ^{10}Be record is sufficiently deep in the core with a large uncertainty on the value of thinning which can easily compensate for changes in accumulation rates. For such an extreme case, the resulted amplitude of the accumulation rate during the glacial–interglacial transition is only different by 28% from the EDC3 one. In

turn, we do not retain this assumption of a constant flux as much as the millennial variability of the ^{10}Be flux derived using the EDC3 accumulation (Fig. 5.1) is rather small and quite comparable with what is observed during the Holocene.

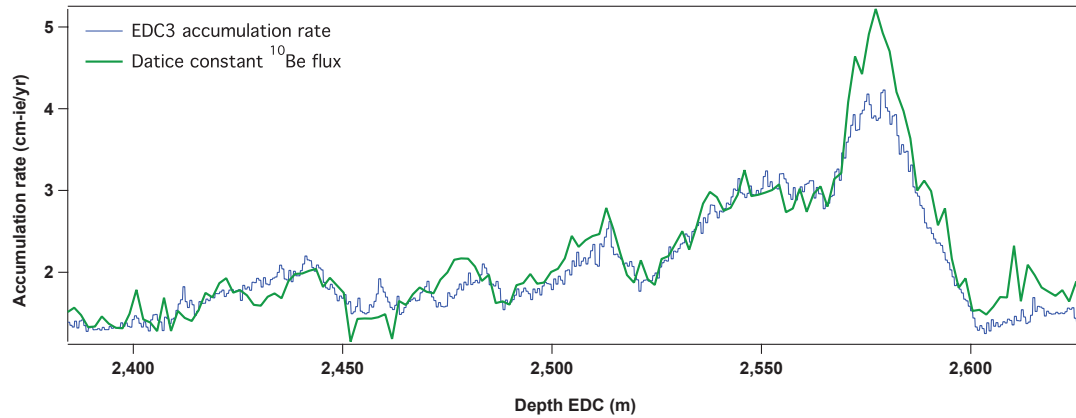


Figure 5.5: Consequences on the accumulation rate of a constant ^{10}Be flux (fixed at $53.44 \text{ at} \cdot \text{m}^{-2} \cdot \text{s}^{-1}$ over the whole period) using the bayesian dating tool Datice [Lemieux-Dudon et al., 2010]. The Datice output curve is in green and the EDC3 accumulation rate in blue.

If the assumption of a strictly constant flux is unrealistic, it is reasonable to expect that this parameter does not show any correlation with δD at the time of glacial-interglacial transition. The relationship between ^{10}Be flux and δD between ~ 340 and 320 kyr BP indeed directly depends on the amplitude of the accumulation change between glacial and interglacial periods. In the formulation adopted by Parrenin et al. [2007a] this accumulation, A , is defined as $A^0 \exp(\beta \Delta \delta D_{smo})$ in which A^0 is the present-day accumulation rate ($2.841 \text{ cm}\cdot\text{ie}/\text{yr}$ at EDC) and $\Delta \delta D_{smo}$ the deviation from the present-day δD values (corrected for the variations in isotope and temperature at the source of the air masses, and 50-yr smoothed). β is an adjustable parameter which is optimized during the construction of the ice core chronology in order to respect thinning and age markers constraints. For example the EDC3 chronology uses a β of 0.0157. Keeping the consistency with age markers, we have searched to adjust β in order to minimize the variance of the signal (which is easily compensated by changes in the thinning function as shown in the previous paragraph). We have limited this search on the time interval from 341 to 319 kyr BP which although encompassing the full amplitude of glacial–interglacial changes, exhibits a small millennial variability. The variance is minimized for an increase by 7% which corresponds to a larger glacial-interglacial amplitude by the same amount (the variance remains around its minimal value for $0.0163 < \beta < 0.0173$). When we apply this increased value of β to our whole record, we also notice a general

decrease of the variance which validates this revision of accumulation rate estimate from δD over one glacial–interglacial cycle. Still, this change in the amplitude of the accumulation rate does not modify the general shape of the ^{10}Be flux record and preserve its spectral properties. Earlier chronologies developed for Antarctic ice cores were based on a different approach, e.g. on the assumption that accumulation changes are driven by the derivative of the saturation pressure, as would be the case in a simple 1D model [Ritz, 1992]. Under this assumption, the accumulation change depends on the temperature change in the atmosphere which is linearly related to surface temperature change, ΔT_s [Jouzel and Merlivat, 1984], itself assumed to be related to δD , $\Delta T = \delta D/\alpha$. With this formulation, the variance of the ^{10}Be flux is minimized for an α value 12% higher than that corresponding to the present-day observed isotope/temperature slope used in the conventional approach known as the “isotopic paleothermometer”. As for the earliest formulation, the variance of the ^{10}Be flux is minimized over the whole period 270 – 355 kyr BP. Despite the limitations of this simple approach, this result gives support to this conventional approach which may however slightly underestimate the estimated glacial-interglacial temperature changes, e.g. by about 10%, a value similar to that derived by Jouzel et al. [2003].

5.5 Link to solar activity cycles

Here we analyze centennial variations recorded in ^{10}Be flux in order to search the signature of solar activity cycles. Several temporal studies of solar activity during the Holocene using cosmogenic nuclide are available in the literature (see section 5.1). The most recent is the one from Steinhilber et al. [2012] who extracted the common solar signal from several ^{10}Be profiles recorded in ice cores and ^{14}C measured in tree rings. They combined them in a composite reconstruction, using the principal component analysis (PCA) as a numerical tool for the last 9400 years, excluding potential climatic effects. In this reconstruction, they evidenced periodic variations that could be linked to the Vries cycle (around 210 years) or the Eddy cycle (around 1000 years).

The interglacial period MIS 9.3 included in our ^{10}Be record is the most similar time domain with the Holocene, with a resolution of 20 years, comparable to the one of Steinhilber et al. [2012] (22 years). We have thus performed the same spectral analyses on the Holocene (last 9400 years) and the MIS 9.3 (between 325 and 336 kyr BP) to search for centennial variability linked to solar activity and to compare the resulting spectra: wavelet analysis and global Fourier spectrum. The wavelet analysis method is well adapted to describe non-stationary periods or changes in

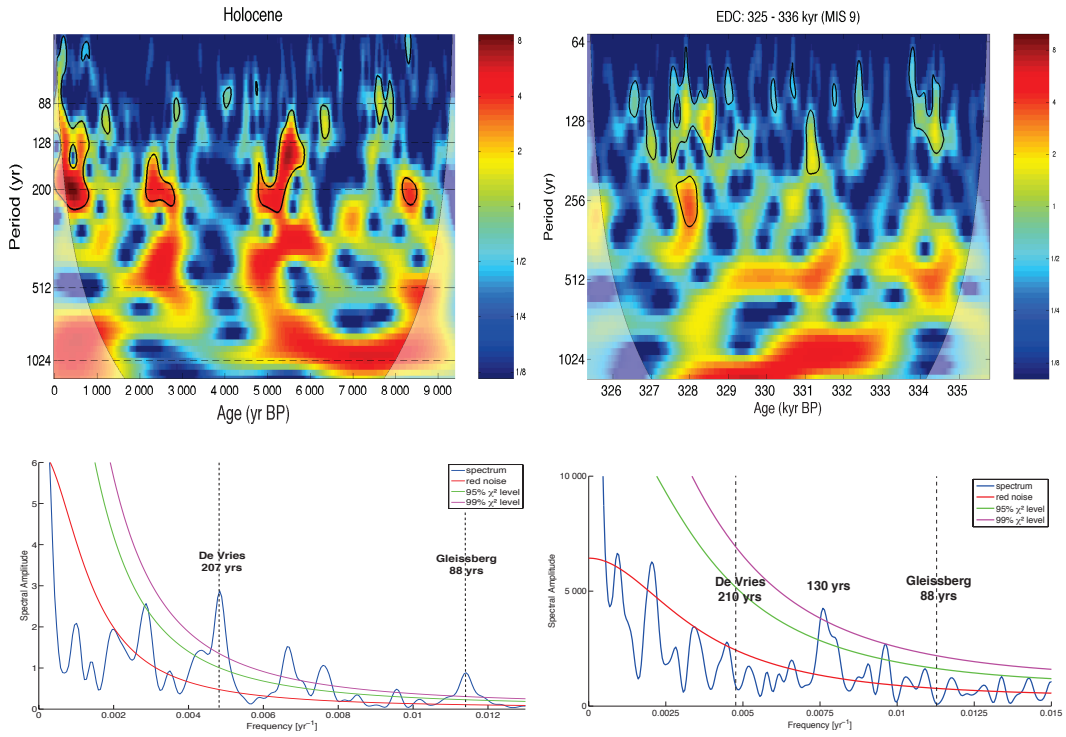


Figure 5.6: Comparison of the spectral analyses (Wavelet and Fourier) of centennial variability during the Holocene with the composite from [Steinhilber et al. \[2012\]](#) (left column) and the interglacial period MIS 9.3 in our ^{10}Be record (right column). The De Vries and Gleissberg cycles are detected during the Holocene but not during the MIS 9.3.

frequency and magnitude, so it is the best tool for our study.

The wavelet and the Fourier spectra for the Holocene composite and the MIS 9.3 ^{10}Be record show very different patterns (Fig. 5.6). [Steinhilber et al. \[2012\]](#) found a significant period of 207 years, considered as the de Vries cycle, located at 0 – 810, 2100 – 2800, 4770 – 5430 and 8180 – 8530 yr BP. Less prominent periodicities such as the Gleissberg cycle (88 years) and others around 150 yr and 130 yr are possibly visible in the spectra. On the contrary, during the MIS 9.3 we detect only a powerless but significant 130 years cycle, over very small time periods (327.5 – 328.7 kyr BP and 333.8 – 334.5 kyr BP), and no sign of the de Vries or Gleissberg cycles. However, one can notice a 92 years period significant at 95% in the Fourier spectrum of our ^{10}Be record during the MIS 9.3, which could be the imprint of the Gleissberg cycle taking into account the uncertainties of the chronology. Note that our results do not depend on the use of ^{10}Be concentrations profile instead of the flux or the use of on different age scales (AICC2012 from [Bazin et al. \[2013\]](#) and DFGT-2006 from [Parrenin et al. \[2007a\]](#)) shows the same trend in the spectra (Fig. 5.7).

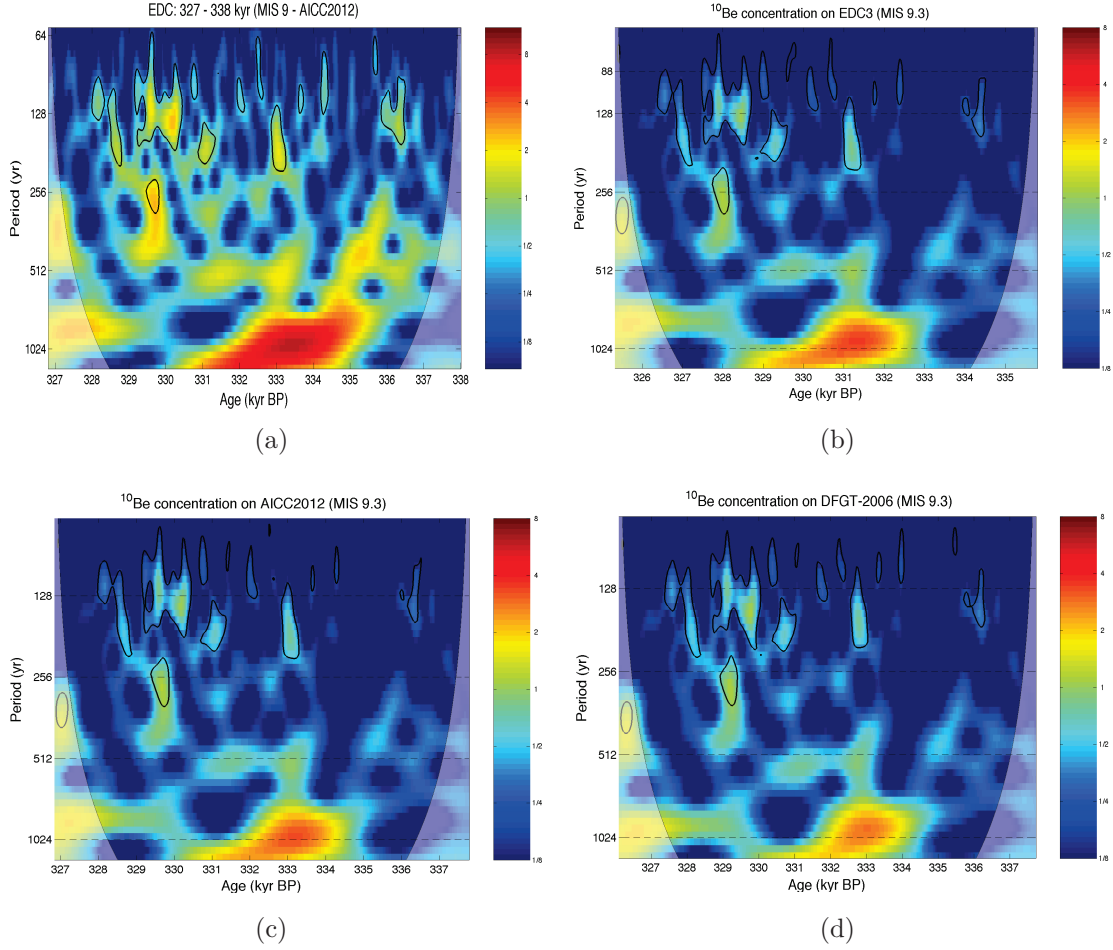


Figure 5.7: Sensitivity tests of the spectral analyses during the MIS 9.3. (a) ^{10}Be flux on the AICC2012 age scale [Bazin et al., 2013]. (b) ^{10}Be concentrations on the EDC3 age scale. (c) ^{10}Be concentrations on the AICC2012 age scale. (d) ^{10}Be concentrations on the DFGT-2006 age scale.

To go further in the comparison between Steinhilber et al. [2012] and our results, the Holocene composite and our ^{10}Be record are not exactly of the same nature. We note that, as a consequence, some climatic effects, normally eliminated in the Holocene composite, could influence our single ^{10}Be record. We have thus isolated the ^{10}Be concentrations record from the EPICA Dronning Maud Land (EDML) ice core (Fig. 5.8) from the Holocene composite from Steinhilber et al. [2012]. This ^{10}Be record looks like the composite from Steinhilber et al. [2012] and is now compared to the spectral analyses of our ^{10}Be profile. On the EDML Holocene ^{10}Be record, we detect the Gleissberg cycle (88 years), during only a short period between 7000 and 8000 yr BP, and the de Vries cycle (210 years), but to a lesser degree than in the spectra of the Holocene composite. These differences may be linked to climatic

effect (e.g. section 5.3) influencing the ^{10}Be flux. Still, even if solar cycles are slightly less obvious on the ^{10}Be at EDML than on the composite curve, there is still the same contrast with the results from the MIS 9.3 period. This is surprising because there is apparently no reason that the solar cycles have been modified between the Holocene and the MIS 9.3.

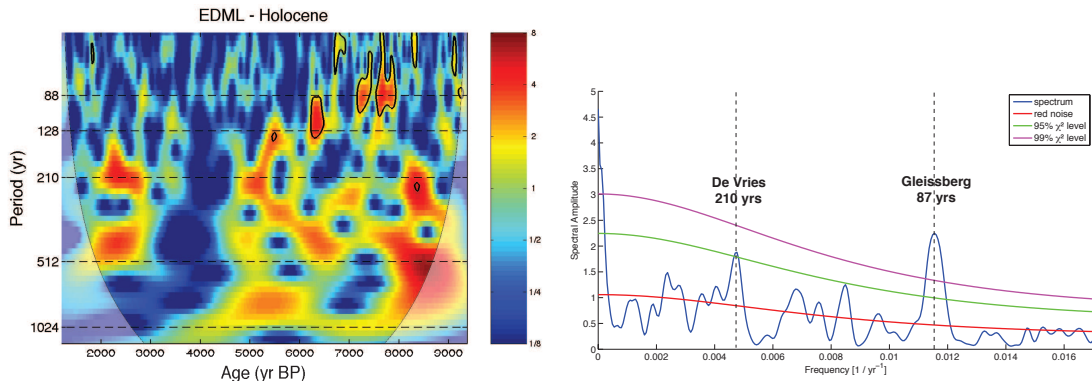


Figure 5.8: Spectral analyses of centennial variability of the ^{10}Be record at EDML during the Holocene [Steinhilber et al., 2012]. They show the same picture as those of the Holocene composite.

Using the same method, we have extended our search for the presence of characteristic periodicities of solar activity (especially the de Vries cycle) over our whole ^{10}Be record and not only over MIS 9.3. For this objective, we performed the temporal analyses on the ^{10}Be flux by step of 10000 years (275 – 285 kyr BP, 285 – 295 kyr BP...). To avoid extrapolation, data are resampled to the lowest resolution of the concerning time interval. The results of the spectral analyses are summarized in the Table 5.1 and the Appendix C.2. We can firstly notice that according to the period studied, the values of the “detected” cycles move from 130 to 250 years, except one centennial period of 625 years in the oldest part of the ice core. The only possible imprint of the de Vries cycle is during the 10000 years after the interglacial period MIS 9.3 (315 – 325 kyr BP interval) where a significant cycle of periodicity 205 years is seen at 316.5 – 316.9, 319 – 320.2 and 321 – 321.6 kyr BP. On the others analyzed time interval, the ^{10}Be record does not show such a periodicity. Finally, we do not place much confidence in the detection of centennial cycles apart from MIS 9.3 because of the lower resolution of our ^{10}Be record in glacial period. Indeed, the resampling of the different time intervals during the glacial period varies between 45 and 69 years. For example, we detect a possible cycle of 180 years (on the intervals 275 – 285, 295 – 305 and 305 – 315 kyr BP) but the resampling performed of our ^{10}Be record for the wavelet analysis is 45-49 years, which leads to a cycle with less

than four points.

Fig.	Time interval (yr BP)	Resampling (yr BP)	Cycle (yr)
5.2	269000 – 355000	70	11000
5.6, left	0 – 9400 (Holocene)	22	88, 130, 150, 208
5.6, right	325000 – 336000 (MIS 9)	29	130
5.8	1200 – 9400 (Holocene)	5	88, 210
C.1a	275000 – 285000	49	180
C.1b	285000 – 295000	45	130, 150
C.1c	295000 – 305000	46	150, 180
C.1d	305000 – 315000	48	180
C.1e	315000 – 325000	45	205
C.1f	335000 – 345000	69	220
C.1g	345000 – 355000	67	625

Table 5.1: Table resuming the results of the spectral analyses. The left column refers to the concerning figure, the second column to the time interval analyzed, the third column to the resampling applied for the wavelet analysis and the right column to centennial cycles detected in the ^{10}Be flux at EDC.

All these results lead us to conclude that we could not easily relate centennial variations in our ^{10}Be record to solar activity periodicity as the de Vries cycle, detected during the Holocene, even during the highly-resolved interglacial period MIS 9.3. Note firstly that even if tests on the chronology (Fig. 5.7) do not show consequent changes on centennial variability of the ^{10}Be record, we cannot exclude uncertainties on the datation. The non detection of the de Vries cycle in our ^{10}Be record raises questions about the long-term stability of solar cycles documented during the Holocene, and so about the recent suggestion of a planetary influence on solar activity by Abreu et al. [2012]. Indeed, because the frequencies of the applied strength on the Sun by the planets should be enough stable on million years at first order (D. Paillard, private communication), we should detect the de Vries cycle during the MIS 9.3 period. But our results lead clearly to a discrepancy regarding this hypothesis of a planetary influence on the modulation of solar activity. Other high resolution cosmogenic isotopes records during older periods than the Holocene are strongly needed to clarify the validity or not of this hypothesis, and to improve our knowledge of centennial periodicities of solar activity.

In addition to centennial variability, the strongest periodicity in the ^{10}Be record is a 10.5 ka cycle (Fig. 5.2) that cannot be explained by climatic influence. These long-term variations exhibits clear minimum evidenced in Fig. 5.1. Within the uncertainties of chronology, the minimum and maximum of ^{10}Be production at 302.8 and 328.21 kyr BP respectively are correlated with the maximum and minimum of

the geomagnetic paleointensity stack PISO-1500 [Channell et al., 2009] at 298 and 321 kyr BP (Fig. 5.9). This confirms the influence of geomagnetic field intensity on long time variations of ^{10}Be flux at EDC and the possibility to compare our ^{10}Be signal with paleomagnetic deep-sea core records. This aspect is discussed in the next chapter along with the contribution of ^{10}Be data to the development of a common chronology between ice cores and deep-sea cores.

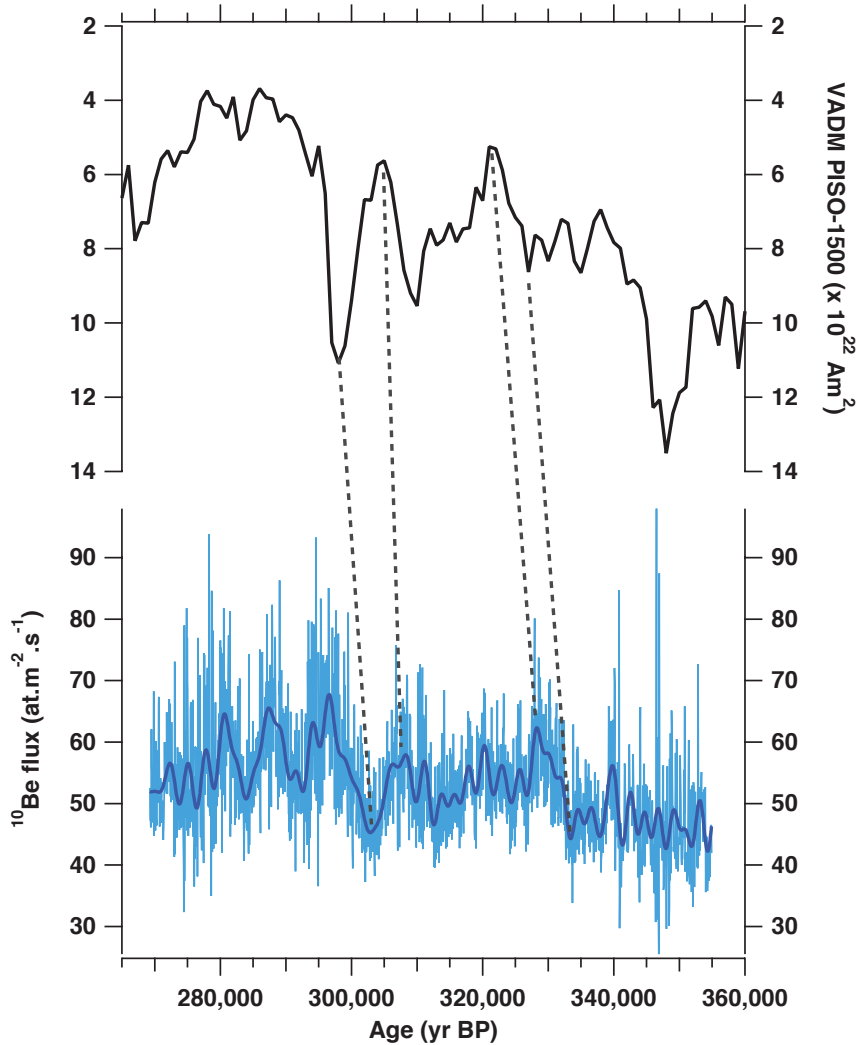


Figure 5.9: Comparison between the Virtual Axial Dipole Moment from the marine stack PISO-1500 (black curve on an inverse scale) [Channell et al., 2009] and the ^{10}Be flux at EDC (raw data : light blue curve; $1/2000\text{yr}^{-1}$ low-pass filtered data: bold blue curve).

5.6 Conclusions

^{10}Be measurements have been performed in the EDC ice core at high resolution (11 cm: between 20 and 70 years on EDC3 age scale) for a whole climatic cycle, including MIS 9.3. We have performed a systematic study of the potential influences on ^{10}Be flux: chronology (accumulation rate and datation), transport and deposition of ^{10}Be , and climate. We cannot rule out that accumulation rate changes explain variations of ^{10}Be flux at EDC because of large uncertainty on thinning determination at this depth and rather weak ^{10}Be variations during this period. There is no correlation between the ^{10}Be flux and climate in the EDC ice core during this climatic cycle and its millennial variations cannot be mainly explained by the influence of transport or deposition. Our record supports the interpretation of glacial–interglacial temperature change based on present-day distribution of water isotopes, with however an underestimation of 10 to 20%.

We have performed several spectral analyses, firstly on the $^{10}\text{Be} + ^{14}\text{C}$ composite during the Holocene period and our high resolution ^{10}Be record, and then on the ^{10}Be record at EDML during the Holocene period, to detect centennial cycles of solar activity. We have detected some centennial variations in our whole ^{10}Be profile but we could not relate them clearly to centennial cycles of solar activity (as the de Vries cycle), even over the interglacial MIS 9.3 period with a 20-yr resolution. This contrast with the 200-yr cycle detected for the Holocene period and questions the long-term stability of solar cycles and the hypothesis of a planetary influence on solar activity. The millennial variability in our ^{10}Be record, most likely resulting from the modulation by the geomagnetic field, is discussed in the following chapter along with the contribution of these data to complete a high resolution continuous record between 200 and 800 kyr BP and to the development of a common chronology between ice cores and marine sediment cores.